Available online at www.sciencedirect.com
ScienceDirect
International Journal of Thermal Sciences 47 (2008) 458–467
International Journal of Thermal Sciences
www.elsevier.com/locate/ijts

Experimental heat transfer and flow analysis of a vented brake rotor

A.D. McPhee, D.A. Johnson *

University of Waterloo, Department of Mechanical Engineering, Waterloo, ON, N2L 3G1, Canada

Received 9 September 2006; received in revised form 8 March 2007; accepted 9 March 2007

Available online 15 May 2007

Abstract

Brake rotors generate an opposing torque to a shaft, converting kinetic energy to heat thus necessitating heat transfer considerations. To better understand convection through the fins of a brake rotor, experimental and analytical methods were employed. The experimental approach involved two aspects, assessment of both heat transfer and fluid motion. A transient experiment was conducted to quantify the internal (fin) convection and external (rotor surface) convection terms for three nominal speeds. For the given experiment, conduction and radiation were determined to be negligible. Rotor rotational speeds of 342, 684, and 1025 [rpm] yielded fin convection heat transfer coefficients of 27.0, 52.7, 78.3 [$\mathrm{W\,m^{-2}\,K^{-1}}$], respectively, indicating a linear relationship. At the slowest speed, the internal convection represented 45.5% of the total heat transfer, increasing to 55.4% at 1025 [rpm]. Analytical solutions were evaluated where possible for the convective terms and found to be comparable to the experimental results. The flow aspect of the experiment involved the determination of the velocity field through the internal passages formed by the radial fins. Utilizing PIV (particle image velocimetry), the phase-averaged velocity field was determined. A number of detrimental flow patterns were observed, notably entrance effects and the presence of recirculation on the suction side of the fins.

Keywords: Brake rotor; Transient experiment; Radial fin; PIV; Forced convective cooling

1. Introduction

The primary function of a brake rotor is to act as a friction surface, generating an opposing torque to a shaft. The automotive and aerospace industries rely on these devices to provide vehicle deceleration. In this application, the brake rotor commonly forms part of the wheel assembly, transferring the opposing torque to the tires of the vehicle. During braking, energy is transferred to the rotor in the form of heat. As a result, the brake rotor must also serve as an efficient energy dissipation and storage device. In most cases, air must be circulated through the rotor to provide adequate cooling. The passages, formed by the radial fins between the braking surfaces, act as a centrifugal fan, facilitating the required air flow for cooling.

To improve the performance of a vented brake rotor, an understanding of flow and heat transfer phenomena is of utmost importance. Of particular interest is the air flow through the passages. While numerical modeling can predict flow and heat transfer characteristics and serve as an efficient design tool, the results are subject to great uncertainty. The experimental approach, however, provides an assessment of actual performance and serves as a critical validation tool to numerical modeling.

Experimental evaluation of a rotor's overall heat transfer performance is frequently performed in research. Dubensky [1], Sisson [2], and Daudi [3] have based experiments on the use of a brake dynamometer. This approach offers an accurate global validation method, however does not offer insight into the individual heat transfer mechanisms. The flow field has also been subject to experimental analysis in the past. Parish et al. [4] used hot wire anemometry and pressure probes at the exit of a vented rotor to quantify mean and turbulent components of the bulk flow.

Past research regarding the design of a thermally efficient brake rotor has often resulted in the use of numerical methods. In studies conducted by Zhang [5,6], the approach was simply to enhance airflow through the radial passages. The inherent deficiency in this method is the absence of any thermal modeling, thus negating heat transfer performance. While the resulting design might demonstrate increased airflow, by not addressing the

* Corresponding author. Tel.: +1 519 888 4567 x33690.
E-mail address: da3johns@uwaterloo.ca (D.A. Johnson).

1290-0729/$ – see front matter
doi:10.1016/j.ijthermalsci.2007.03.006

Nomenclature

A	Surface area	m^2	
a, b	Exponential curve fit constants		
c	Specific heat	$J\,kg^{-1}\,K^{-1}$	
$\dot{E}$	Rate of energy	$J\,s^{-1}$	
h	Heat transfer coefficient	$W\,m^{-2}\,K^{-1}$	
k	Thermal conductivity	$W\,m^{-1}\,K^{-1}$	
k_t	Turbulent kinetic energy (TKE)	$m^2\,s^{-2}$	
l_c	Length scale	m	
m	Mass	kg	
N	Rotor speed	rpm	
$\bar{N}$	Rotor speed, time-averaged	rpm	
Q	Volume flow rate	$m^3\,s^{-1}$	
Re	Reynolds number		
t	Time	s	
T	Surface temperature	K	
T_0	Initial temperature	K	
T_∞	Ambient temperature	K	
U	Overall heat transfer coefficient	$W\,m^{-2}\,K^{-1}$	
$\vec{V}$	Absolute velocity vector	$m\,s^{-1}$	
$\vec{W}$	Relative velocity vector	$m\,s^{-1}$	
$\overline{w^2}$	Relative velocity mean square	$m^2\,s^{-2}$	

Greek symbols

β	Inflow angle	
ϵ	Surface emissivity	
θ	Non-dimensional temperature	
σ	Stefan–Boltzmann constant	$W\,m^{-2}\,K^{-4}$

Subscripts

cond	Conduction
conv	Convection
e	External surfaces
exp	Experimental
hub	Rotor hub
i	Internal (passage) surfaces
out	Exiting the surface
rad	Radiation
RMS	Root mean square
st	Stored in the volume
the	Theoretical
x, y, z	Coordinates

effect of turbulence and other such flow parameters, it does not guarantee increased convection.

Improved numerical models have been implemented, including the effects of heat transfer, as demonstrated by Phan et al. [7], Jones et al. [8], and Shen et al. [9]. Numerical models, however, are often subject to significant assumptions. Correlations to the experimental data have often relied on the bulk performance in terms of heat transfer coefficients, rather than consideration of an accurate flow field and addressing specific phenomena.

The purpose of this experiment will be to characterize the individual heat transfer mechanisms through transient testing. This experiment will also evaluate the fluid motion through the radial passages of the brake rotor using PIV (particle image velocimetry). Using the results of the heat transfer and PIV experiments, the potential for accurate numerical modeling becomes possible. Such a model could then be expanded to consider the interaction with other vehicle components, such as the wheel hub, caliper and shroud, accurately predicting in-vehicle heat transfer performance.

2. Heat transfer

2.1. Physical mechanisms

The evaluation of heat transfer requires consideration of the individual contributing mechanisms, which for a brake rotor involves conduction, convection, and radiation. In terms of convective heat transfer, the mechanism can be considered in two parts. The first involves convection from all external surfaces. The second, and of particular interest, involves convection through the radial passages. Assuming constant surface temperature and mean heat transfer coefficients, the convective terms are defined as follows [10]:

$$\dot{E}_{\text{conv.e}} = h_{\text{conv.e}} A_{\text{e}} (T - T_\infty) \tag{1}$$

$$\dot{E}_{\text{conv.i}} = h_{\text{conv.i}} A_{\text{i}} (T - T_\infty) \tag{2}$$

For this experiment, characterization of the aforementioned convective heat transfer terms was desired. Thus, the aim was to minimize the remaining heat transfer mechanisms, conduction (accounting for contact resistance) and radiation [10]:

$$\dot{E}_{\text{cond}} = U_{\text{cond}} A_{\text{hub}} (T - T_\infty) \tag{3}$$

$$\dot{E}_{\text{rad}} = h_{\text{rad}} A_{\text{e}} (T - T_\infty) \tag{4}$$

$$h_{\text{rad}} \equiv \epsilon\sigma (T + T_\infty)\left(T^2 + T_\infty^2\right) \tag{5}$$

Conduction, which occurs through the mounting hub, was minimized through the use of an asbestos disc between the two mating surfaces, thus insulating the brake rotor. In an effort to reduce the radiation contribution, experimental operating temperatures were limited, as radiation is a function of T^4. Evaluation of these assumptions will be provided during the analysis of the results. Neglecting conduction and radiation terms, the total heat transfer can then be expressed in terms of convection alone:

$$\dot{E}_{\text{out}} = \dot{E}_{\text{conv.i}} + \dot{E}_{\text{conv.e}} \tag{6}$$

To quantify the rate of heat transfer, it was desired to conduct a transient experiment. Applying an energy control volume analysis to the surface of the brake rotor, the rate of change of internal (stored) energy is defined as:

$$\dot{E}_{\text{st}} = -\dot{E}_{\text{out}} \tag{7}$$

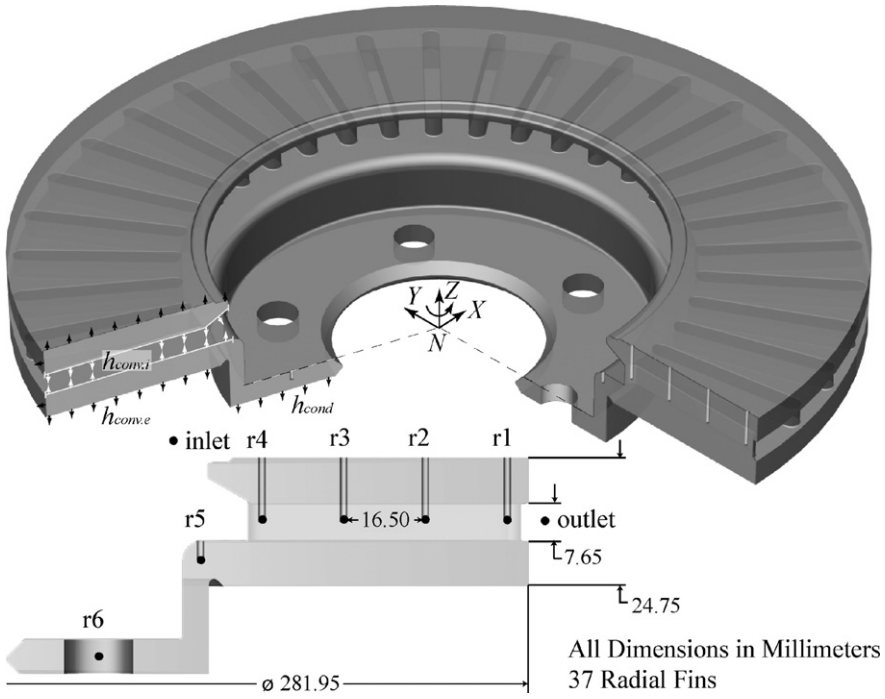

Fig. 1. Rotor geometry and thermocouple placement.

2.2. Lumped capacitance model

To further analysis and to quantify the energy storage term, use of the lumped capacitance model was desired, in part due to its simplicity. The lumped capacitance model is based on the assumption that the temperature of the solid is spatially uniform at all times during a transient process [10]. This simplification eliminates any spatial terms from the energy storage expression, and can be expressed as [10]:

$$\dot{E}_{\mathrm{st}} = mc\frac{\mathrm{d}T}{\mathrm{d}t} \tag{8}$$

To ensure the validity of this assumption, the following requirement for the Biot number needed to be satisfied [10]:

$$Bi = \frac{hl_{\mathrm{c}}}{k} \leqslant 0.1 \tag{9}$$

In Eq. (9), a conservative estimate was used for h based on initial test results, while k was defined by the material properties. Two methods exist for the determination of characteristic length l_{c}. The first, and most common approach, is to calculate the length as the ratio of volume to surface area. The second, and more conservative approach, is to choose l_{c} to be the length corresponding to the maximum spatial temperature difference. For the given rotor geometry, this corresponds to the mid-plane lying between the two pad surfaces, a distance of 0.012 [m]. The first and second method for determining the characteristic lengths yielded Bi values of 0.004 and 0.010, respectively, validating the uniform spatial temperature distribution assumption.

Referring back to the control volume energy balance (7), and substituting for the energy storage term (8), the lumped capacitance model yields the following solution [10]:

$$\frac{T - T_\infty}{T_0 - T_\infty} \equiv \theta = \exp\left[-\frac{h_{\mathrm{conv,i}}A_{\mathrm{i}} + h_{\mathrm{conv,e}}A_{\mathrm{e}}}{mc}t\right] \tag{10}$$

Utilizing the preceding result, the heat transfer coefficients can readily be determined by conducting a transient experiment.

2.3. Experiment

For the experiment, a generic 37-radial fin vented brake rotor was utilized as illustrated in Fig. 1. The rotor was fabricated from cast iron with a mass of 7.36 [kg] and specific heat of 566 [$\mathrm{J\,kg^{-1}\,K^{-1}}$] [10]. The external and internal convective areas were determined to be 0.120 and 0.102 [$\mathrm{m^2}$], respectively.

For each of the experiments, the brake rotor was heated to a uniform temperature of 583 [K] over a period of 45 minutes. A maximum temperature of 583 [K] was selected to minimize the radiation and conduction heat transfer mechanisms. Furthermore, heating over a long period ensured spatial uniformity for the temperature distribution. To facilitate heating of the brake rotor, a 5.5 kW induction heater was utilized, ensuring a spatially uniform temperature distribution. A custom induction coil was fabricated to accommodate the rotor geometry. During the heating process, the rotor was slowly rotated to ensure uniform heating.

Upon reaching the desired temperature, the heat source was removed and the brake rotor accelerated to a constant speed. A custom test bench was fabricated to facilitate the rotation of the brake rotor, simulating in vehicle operation. The rotor was driven by a 1 [hp] DC motor, with speed controlled by an open-loop variable resistance drive. The rotor was attached to the motor via a hub assembly, with any obstructing shrouds removed. The inlet of the rotor faced outward from the hub, preventing any potential obstructions. The resulting setup best simulated the performance of an unobstructed brake rotor open to the atmosphere. The temperature decay of the brake rotor was monitored until a temperature of 323 [K] was reached and

subsequently used to determine the heat transfer coefficients for a given speed.

Acquisition of brake rotor temperatures was accomplished using K-type thermocouples. While infrared (IR) imaging presents a less intrusive method of temperature acquisition, mounting the thermocouples directly to the brake rotor required less post-processing while providing greater accuracy and excellent response. As such, the measurement error appearing in the results is minimal compared to the assumption of negligible conduction and radiation. Eight thermocouple locations were determined during initial stages of testing, the locations of which are specified in Fig. 1. This was considered adequate for capturing the spatial temperature distribution of the brake rotor. Four of the eight thermocouples (r1–r4) were placed at the mid-plane of the fin through 1.5 [mm] holes drilled from the pad surface. A sodium-silicate based cement was used to hold the thermocouples in place, ensuring high thermal-conductivity. The remaining thermocouples were used to measure the temperature of the outer (r5) and inner (r6) portions of the mounting hat, as well as the inlet and outlet air temperature.

To accommodate data acquisition for the seven thermocouples fixed to the rotating assembly, an eight channel slip ring (Michigan Scientific) was used. The remaining thermocouples, exit air and ambient, were fixed in space. An encoder mounted to the rotor shaft facilitated measurement of the rotor speed. Data acquisition was accomplished using a Keithley 2700 datalogger and sampled on all channels at a rate of 1 [Hz]. Due to the thermal inertia of the brake rotor, a sampling rate of 1 [Hz] was considered more than sufficient.

Initially, the experiment was conducted for the brake rotor with the vented portion blocked. This was accomplished by covering the entry and exit of the radial passages with adhesive aluminum tape. Doing so eliminated the internal convective heat transfer, permitting the external convection term to be determined. Knowing the external convective heat transfer, the experiment was conducted for the open brake rotor, from which the internal convection was determined. The experiment was conducted for three nominal speeds of 342, 684, and 1025 [rpm], corresponding to typical vehicle operating speeds.

2.4. Results

In conducting the experiments for the blocked and open vented rotor, it was desired to operate at exactly 342, 684, and 1025 [rpm]. The actual speeds, however, varied slightly from these nominal speeds. The mean and RMS values for each are listed in Table 1.

The results of the first experiment, for the blocked rotor at 342 [rpm], are shown in Fig. 2. Given that the vented portion was blocked, the inlet and outlet temperatures have no bearing on the results and have been omitted from the figure. Observation of Fig. 2 illustrates a number of points. Firstly, the two thermocouples on the mounting hat portion of the brake rotor, r5 and r6, measured temperatures 10–25% lower than the finned section. This spatial variation was in part due to the induction heating occurring at the finned section as well as the minor conduction occurring through the hub. While the conduction mechanism is small it appears deceivingly large, a result of the reduced thermal mass of the mounting hat. Given that the first experiment represents the poorest convective heat transfer performance, the conduction error presented represents a maximum for the study. Given the small thermal mass, the minimal convection occurring at that surface, and the decrease of spatial variation with time, this deviation was considered negligible.

Table 1
Actual mean and RMS rotor speeds

N [rpm]	Blocked		Open	
	$\bar{N}$	N_{RMS}	$\bar{N}$	N_{RMS}
342	340.3	4.3	342.1	3.1
684	674.9	8.3	676.6	8.1
1025	1013.4	7.7	1016.9	7.3

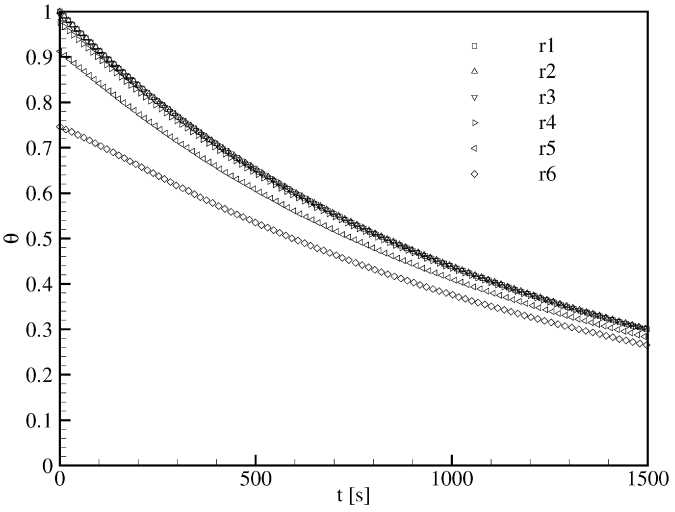

Fig. 2. Non-dimensionalized temperature vs time for blocked vented rotor at 342 [rpm].

The convection terms are largely dependent on the temperature of the finned section. In this region, the experimental data exhibited a maximum of 2.4% deviation between the four thermocouples, thus exhibiting excellent spatial uniformity. Much of the initial deviation was a product of the induction heater, and quickly decayed with increasing time.

Proceeding with data from the finned section, Fig. 3 contains a plot for the four locations. This plot clearly illustrates that the temperature assumes an exponential decay, as predicted by Eq. (10). Applying an exponential curve fit, the results for the given experiment are tabulated in Fig. 3, and assume the following form:

$$\theta = a\mathrm{e}^{-bt} \tag{11}$$

The exponential curve fit for each of the four locations yielded similar results. In all cases, the leading coefficient a was less than the expected value of unity. This less than unity value resulted from the minor conduction occurring through the hub. The deviation from unity, however, was minor, and since convection was a minimum for this test scenario, the deviation will be less pronounced for the remaining test cases.

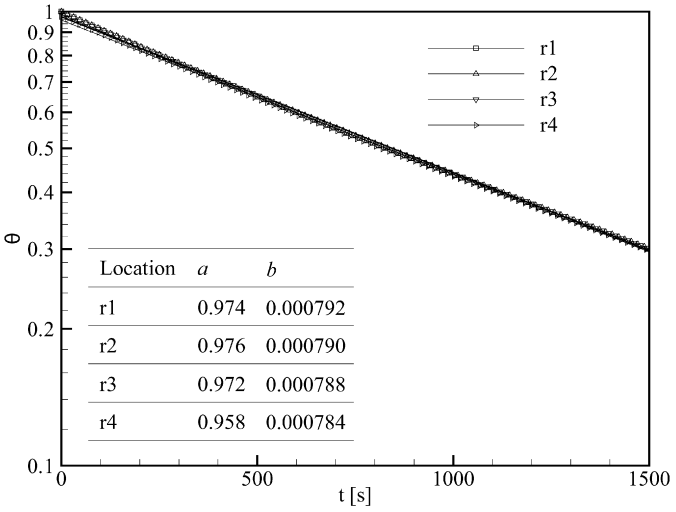

Fig. 3. Non-dimensionalized temperature vs time for blocked vented rotor at 342 [rpm] (log plot).

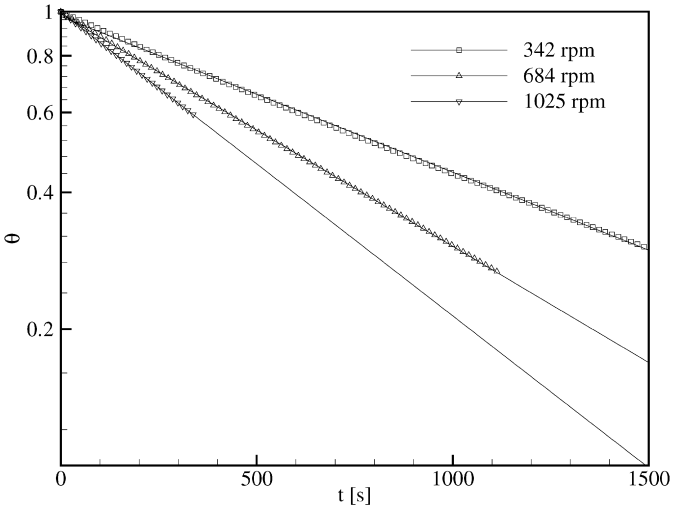

Fig. 4. Non-dimensionalized temperature vs time for blocked vented rotor at various speeds (r2 location).

Table 2
Exponential curve fit and external convective heat transfer coefficients for blocked vented rotor

N [rpm]	b	$h_{\text{conv.e}}$ [$\text{W m}^{-2}\,\text{K}^{-1}$]
342	0.000789	27.4
684	0.001176	40.8
1025	0.001535	53.3

Selecting the r2 location for comparison, the results for the blocked vented rotor at the three nominal speeds are presented in Fig. 4. Once again, the correlation between the sample data and the exponential curve fit validates the relationship predicted by Eq. (10). As expected, the temperature decay occurs more rapidly with increasing speed, indicated by the greater slope.

The mean exponential curve fit constants for each speed are presented in Table 2. Proceeding with the exponential constants for the blocked rotor, $h_{\text{conv.e}}$ was determined using Eq. (10) with the results summarized in Table 2.

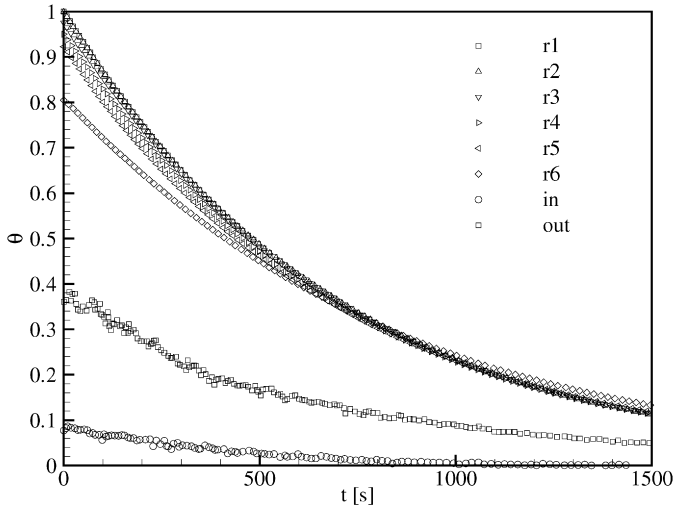

Fig. 5. Non-dimensionalized temperature vs time for open vented rotor at 342 [rpm].

With the external convective heat transfer coefficients determined, the experiment was conducted for the open vented rotor. The results for 342 [rpm], shown in Fig. 5, exhibit a similar exponential decay to that observed with the blocked rotor. The open rotor, however, shows a more rapid decay, as expected with the addition of the internal convective heat transfer. The spatial temperature variance was also reduced, a consequence of the increased convection. The temperature of the mounting surface (r6) exhibits a change in trend, a consequence of the finned section temperature decreasing below the supporting hub and conduction occurring in the opposite direction. Fig. 5 also presents the inlet and outlet temperatures which, unlike the measurements of the thermally large brake rotor, exhibit fluctuations indicative of an unsteady gas flow. The inlet temperature exhibits a 9% increase above the assumed ambient inlet condition, attributed to a portion of the entrained air passing over the external convective surfaces. Since the preheating of the inlet air results from external convection, the total convection is conserved and relations based on the ambient temperature remain valid. This deviation in inlet temperature also quickly decays to ambient. The temperature of the air was increased significantly through the passage, with an initial maximum increase of 38%, decaying exponentially.

Fig. 6 illustrates the excellent spatial uniformity between the four locations, as well as the conformance of the experimental data to the exponential curve fit. The resulting constants for the open vented rotor at 342 [rpm] are also presented in Fig. 6. While the first three locations are much closer to unity, the fourth location remains unchanged due to its close proximity to the conductive surface. The error, however, is minor relative to the dominant convective terms. The exponential constant b exhibits little variation between locations, similar to that observed with the blocked rotor.

Once again selecting the r2 location for comparison, the results for all three nominal speeds are presented in Fig. 7. As with the blocked rotor, the sample data correlates well to the exponential curve fit. The mean curve fit constants for each speed are presented in Table 3. Using Eq. (10) and the external heat

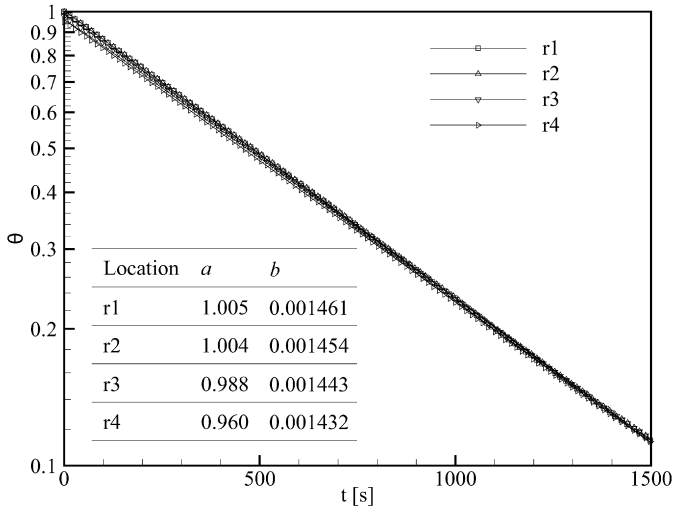

Fig. 6. Non-dimensionalized temperature vs time for open vented rotor at 342 [rpm] (log plot).

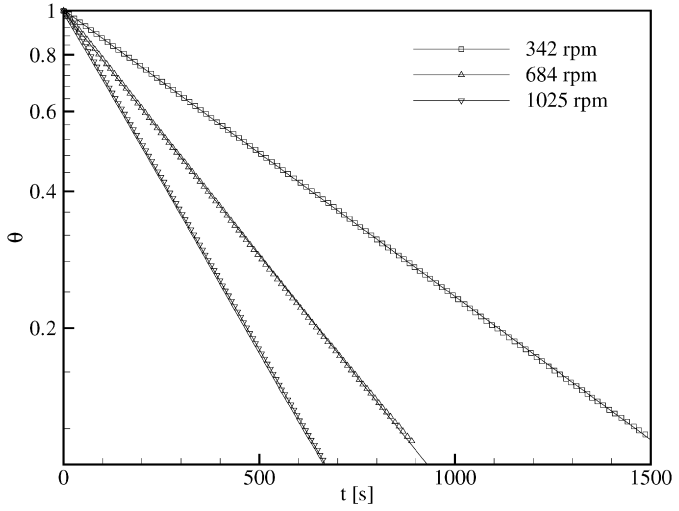

Fig. 7. Non-dimensionalized temperature vs time for open vented rotor at various speeds (r2 location).

Table 3
Exponential curve fit and internal convective heat transfer coefficients for open vented rotor

N [rpm]	b	$h_{\text{conv,i}}$ [$\text{W m}^{-2}\,\text{K}^{-1}$]
342	0.001448	27.0
684	0.002461	52.7
1025	0.003442	78.3

transfer coefficients from Table 2, the internal heat transfer coefficients were determined and are presented in Table 3.

Using the results from Table 2 and 3, Fig. 8 shows the heat transfer coefficient versus rotor speed. While only based on three data points, the sample data correlates well with a linear fit. Unlike external convection, natural convection for the given test setup would be negligible for the internal flow, due to the horizontal orientation of the rotor. Therefore, for zero rotation, the linear fit predicts zero heat transfer, as would be expected for convection with zero flow rate. Thus, for the range of

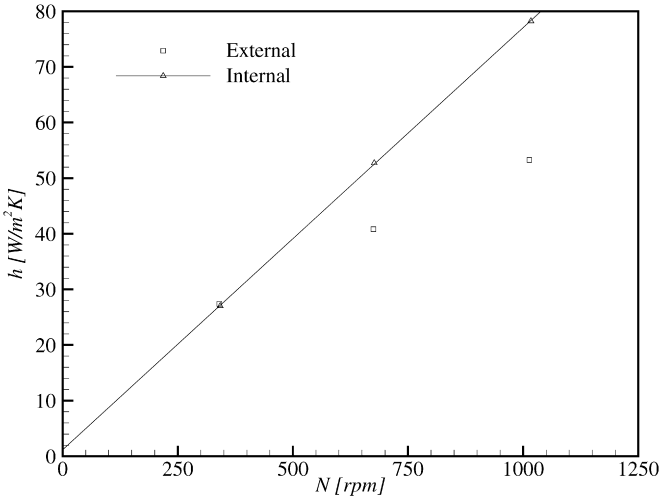

Fig. 8. Heat transfer coefficient versus rotor speed.

speeds tested, internal convection increases linearly with speed. Observation of the external convective term proved less conclusive. Extrapolation of a linear fit for zero rotation yielded a heat transfer coefficient of 14 [$\text{W m}^{-2}\,\text{K}^{-1}$]. While the zero rotation heat transfer coefficient cannot be validated, a non-zero value was to be expected. Given the operating temperature of the brake rotor, the external convective term actually comprises of forced and natural convection. Thus, at zero rotation, convective heat transfer would occur by means of natural convection. However, since the natural convection was not quantified during the experiment, nothing can be stated regarding the linearity of the external convective heat transfer.

Comparing the two convective mechanisms in Fig. 8, the heat transfer coefficients assume similar values at 342 [rpm]. Above this speed, however, the internal convection increases much more rapidly. Taking into account the convective area, the internal heat transfer represents 45.5% of the convective heat transfer at 342 [rpm], increasing to 55.4% at 1025 [rpm]. This result illustrates the importance of vented brake rotors in applications involving moderate speeds above 342 [rpm].

2.5. Analytical comparison

To validate the experimental results, it was desired to evaluate analytical relations where permitted. While the entire brake rotor represents a very complex geometry, the external convection can readily be determined by considering a solid rotating disk. Sparrow and Gregg [11] present an analytical solution for the convective heat transfer from a rotating disk to a fluid. For their analysis, the flow was specified to be laminar while the disk was assumed isothermal and immersed in a large volume of quiescent fluid. The resulting analytical expressions were evaluated numerically for a range of Prandtl numbers. The solution states that the external convective heat transfer is proportional to the root of the speed, confirming the non-linear relationship. Based on the operating conditions and geometry of the disc, the results of the analytical solution are presented in Table 4. For a rotational speed of 342 [rpm], the analytical and experimental result correlated well, with 12.7% error. This con-

Table 4
Experimental and theoretical external convective heat transfer coefficients

N [rpm]	h_{exp} [W m^{-2} K^{-1}]	h_{the} [W m^{-2} K^{-1}]
342	27.4	23.9
684	40.8	33.8
1025	53.3	41.4

firms the minimal impact associated with the conduction and radiation assumptions. The error associated with the analytical solution increased with speed, contrary to the decreasing trend associated with the conduction and radiation assumption. This deviation is likely due to the solution being prescribed for laminar flow, as it does not account for the enhanced convection resulting from the increasing boundary layer turbulence. Thus, the induced error is a result of the simplicity of the analytical model and has no bearing on the accuracy of the experimental results.

2.6. Conduction and radiation assumptions

The conductive heat transfer was shown to be minimal during testing, as indicated by the near unity coefficients for the exponential curve fits. However, to solidify this assumption, the conductive heat transfer can be evaluated using Eq. (3). Based on the thermal conductivity and contact resistance of the 6.35 [mm] asbestos disc, the heat transfer coefficient was determined to be 0.51 [W m^{-2} K^{-1}]. To evaluate Eq. (3), the temperature difference between the mounting hat and hub was required, representing a maximum at t_0. During testing, an initial hub temperature of 438 [K] was recorded. Since both conduction and radiation are independent of rotor speed, the values would assume a maximum percentage of total heat transfer for 342 [rpm]. With an initial mounting hat temperature of 526 [K] for 342 [rpm], the maximum conductive heat transfer was determined to be 44.8 [W]. Based on the experimentally determined heat transfer coefficient, the total heat transfer is calculated to be 1725.2 [W]. Therefore, at most, conduction represents 2.6% of the total heat transfer.

Proceeding with a similar analysis for radiation, Eq. (4) was evaluated. Specifying an emissivity of 0.22 [12] for the cast iron rotor, the maximum radiation heat transfer, corresponding to 583 [K], was calculated to be 161.8 [W]. At 342 [rpm], the radiation component corresponded to 9.4% of the total heat transfer. However, due to the fourth power dependency on surface temperature, the radiation contribution decayed very rapidly with time. This discrepancy could partially account for the predicted non-zero external convection for zero rotation, which has largely been attributed to natural convection.

While the conduction and radiation components represent non-negligible contributions at maximum temperatures and 342 [rpm], the impact quickly decays with time. Also, the contribution at 684 and 1025 [rpm] is much less significant due to the enhanced convective heat transfer coefficients. Thus, the assumption of negligible conduction and radiation has been validated.

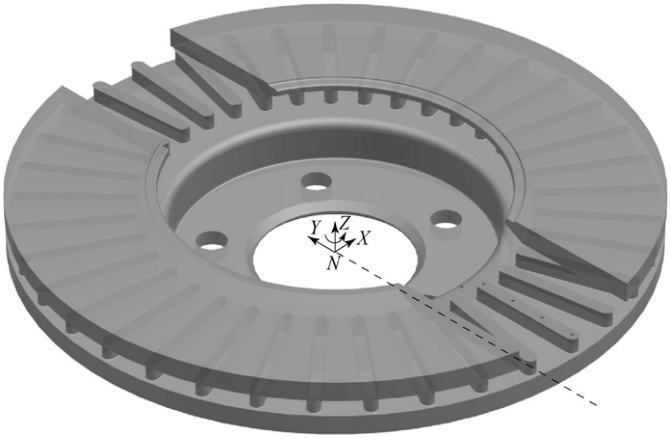

Fig. 9. Modified brake rotor for PIV measurements.

3. Fluid motion

3.1. Experiment

To provide greater insight into the internal convective heat transfer, it was desired to both visualize the flow field and quantify mean and turbulent properties. To accomplish these results, with great accuracy, PIV (particle imaging velocimetry) was utilized.

In this experiment, the test setup from the heat transfer experiment was used to rotate an identical rotor. However, to visualize the flow field of the internal passages, acrylic windows have been installed on the brake rotor as illustrated in Fig. 9. For complexity reasons, the rotor was not subject to heating for the PIV measurements. Rather, the flow field was observed under ambient conditions.

To obtain PIV measurements, illumination of the flow through the passages was provided by a pulsed laser sheet 1–2 mm in thickness, generated by a dual cavity Nd-YAG laser. Vaporized mineral oil was utilized as a seeding particle, to aid in the visualization of the flow. To contain the seeding particles, a large acrylic box surrounded the assembly during testing. For a single acquisition, two images were captured in rapid succession using a Kodak Megaplus ES 1.0 CCD camera with a resolution of 1008 × 1018 pixels, covering an area of 63 by 63 [mm]. Images were processed using cross-correlation, yielding an instantaneous vector field measuring 62 by 62 data points. Johnson et al. [13] provides a detailed description of the PIV setup, cross-correlation routines, and experimental uncertainty.

Similar to the heat transfer experiment, the PIV measurements were conducted for three nominal speeds of 342, 684, and 1025 [rpm]. For each, 500 phase locked instantaneous vector fields were acquired permitting accurate determination of mean and turbulent flow quantities.

3.2. Results

The velocities returned from the PIV experiments represent the absolute motion of the fluid, as the velocity measurements were acquired from a fixed imaging sensor. To analyze the re-

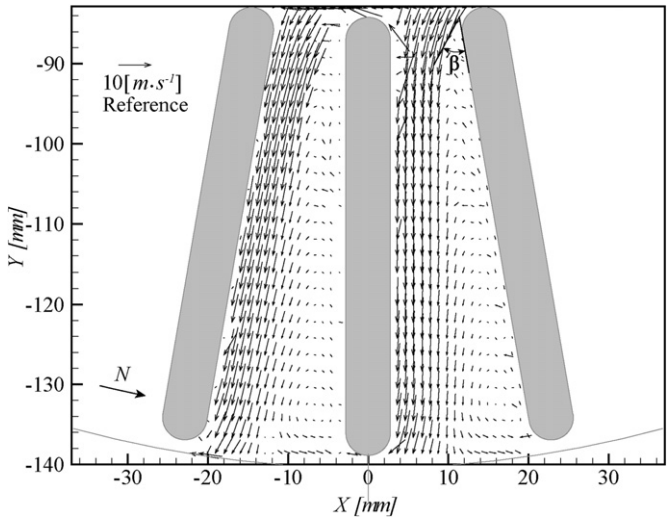

Fig. 10. Phase-averaged relative velocity field for vented brake rotor at 684 [rpm] (counter-clockwise rotation).

sults, it was desired to observe the motion relative to the rotating passages. Using the rotor speed, the relative velocity components were determined.

For each of the three speeds, the resulting velocity fields exhibit similar flow characteristics. The only strong distinction between the velocity fields was the increase in the velocity W_y with increasing rotor speed. The results for the intermediate speed of 684 [rpm], subject to counter-clockwise rotation, are presented in Fig. 10. Due to the counter-clockwise rotation, the left side of the passage is subject to high pressure relative to the right. As such, the left and right sides will be referred to as the pressure and suction sides, respectively.

Fig. 10 illustrates a number of important flow phenomena. For all three test speeds the flow separated from the surface at the leading edge, evident by the flow moving radially inward near the suction surface. This was a result of the large inflow angle β, defined as the angle formed between the velocity vector and suction surface at the leading edge. This back flow resulted in a region of recirculation of slow moving fluid, consuming a large portion of the passage. The impact of this recirculation region is two fold. First, the recirculation hinders the radial flow outward, reducing the mean flow through the passage. Second, the slow moving fluid severely impacts convection occurring at the suction surface. Elimination or reduction of this recirculation region would improve the mean flow and utilize the suction side more efficiently for convection. As previously mentioned, the inflow angle serves as the root cause of the flow separation. As such, any attempt to reduce the angle would delay separation and theoretically reduce this detrimental effect.

Flow along the pressure side of the fin was predictable with a dominant radial velocity component. The substantial increase in velocity at the pressure side relative to the suction side indicates that convection would be greatest along the pressure side. In the heat transfer experiment, this might have been indicated by the presence of an angular temperature gradient. However, due to the radial placement of the thermocouples, an angular gradient was not able to be resolved.

Table 5
Average cross-sectional velocity at exit and total volume flow rate for various rotor speeds

N [rpm]	$\bar{W}_y$ [m s^{-1}]	Q [m^3 s^{-1}]
342	1.6	0.0074
684	3.4	0.0156
1025	4.6	0.0212

Proceeding with the mean velocities, the Reynolds number (Re) for the lowest test speed was calculated to be 1390, well within the laminar regime, increasing to a maximum Re of 3990. Given that the flow field was observed under ambient conditions, the elevated temperatures associated with the heat transfer experiment would result in a change in kinematic viscosity. Accounting for this effect, the corresponding Re values are approximately one-third of those calculated for ambient. As such, laminar flow structures may not be entirely represented in the results. However, given that the flow structures exhibit little change over a significant range of Re, it is unlikely that the observed phenomena would changed appreciably.

In attempts to further the relationship between flow rate and heat transfer coefficients, the velocity data was used to determine the volume flow rate through the rotor. This was accomplished by evaluating the relative velocity vectors near the exit of the passage. In addition to maximizing the quantity of data, data in the exit region was well correlated based on the results of the PIV cross-correlation. Selecting a line of constant y, the normal velocities (W_y) lying between the two fins were averaged over 16 data points. The average was determined using the results for the two resolved passages. The mean velocity, passage area corresponding to the y location, and number of passages were used to determine the total volume flow rate. The flow rate was determined for each of the rotor speeds with the results summarized in Table 5.

Based on the limited number of tested rotor speeds and averaged data points, no definitive statements can result from the volume flow rates. It can be inferred, however, that the resulting flow rate varies linearly with rotor rpm, as illustrated in Fig. 11. This result is identical to the linear relationship obtained for the heat transfer coefficients. While this confirms the presence of a relationship between volume flow rate and convection, it does not guarantee a direct relationship. For example, an increase in volume flow rate might act to increase turbulent kinetic energy (TKE), subsequently enhancing convection. This point illustrates that when dealing with designs subject to different turbulence kinetic energies, the design with the higher volume flow rate may not facilitate greater convection.

Using the fluctuating components resolved during the PIV experiments, the local TKE was defined as follows [14]:

$$k_t = \frac{1}{2}\left(\overline{w_x^2} + \overline{w_y^2} + \overline{w_z^2}\right) \tag{12}$$

In Eq. (12), since the fluctuating component w_z was not resolved by the two-dimensional PIV measurements, the magnitude was approximated by using the non-dominant flow direction component, w_x. Similar to the velocity field, the character-

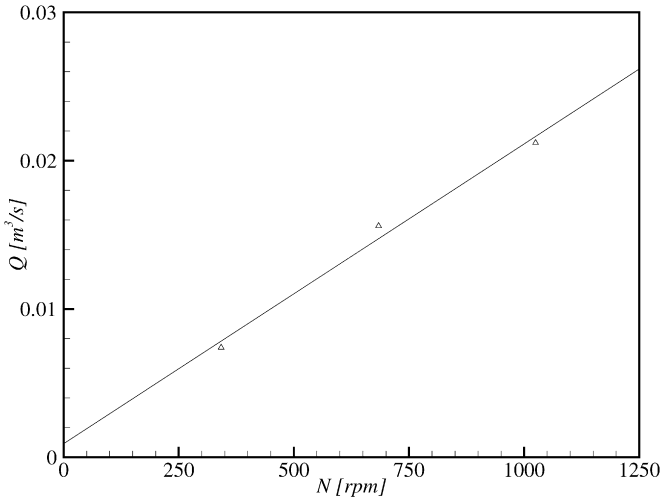

Fig. 11. Volume flow rate versus rotor speed.

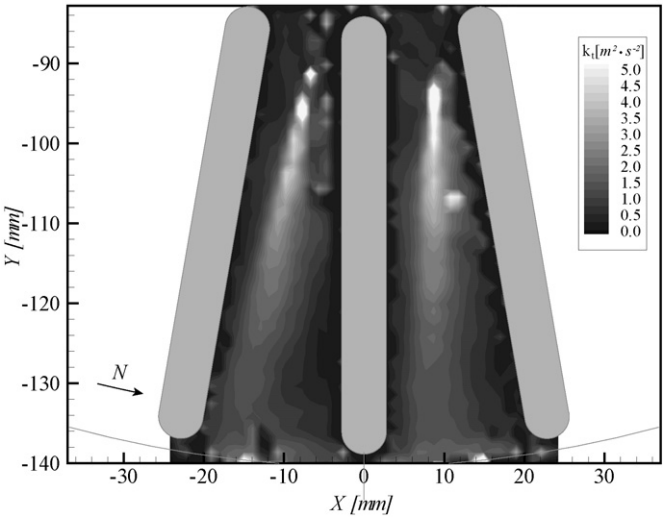

Fig. 12. Turbulent kinetic energy field for vented brake rotor at 684 [rpm] (counter-clockwise rotation).

istics of the TKE field remained similar for all three speeds. The only prominent change between the TKE fields was the increase in magnitude with speed. Fig. 12 illustrates the TKE for the test case of 684 [rpm].

In Fig. 12, the presence of a TKE core is prominent and located along the boundary of the recirculated flow. The generation of the TKE core results from the separation at the leading edge. Extending radially, decreased production as well as dissipation act to reduce the magnitude of the TKE.

Due to the faster flow at the pressure side, the TKE core does not expand rapidly. Also, the recirculation region, which exhibits low velocities, has a vast region of negligible TKE. As a result, the generated turbulence marginally assists in the convection process at the pressure and suction surfaces. The design could be improved by enhancing the expansion of the TKE core, promoting convection at the surface. Enhanced convection would also result from addressing the void which exists in the recirculation region. Aside from the pressure and suction surfaces, the increased turbulence may significantly enhance in-plane convection, as those surfaces benefit from reduced flow separation and zero divergence.

4. Conclusions

To characterize the convective heat transfer for a brake rotor, transient experiments were conducted over a range of rotor speeds. The temperature profiles for each of the nominal speeds conformed to the anticipated exponential decay. Using exponential curve fits generated from blocked rotor testing, the external heat transfer coefficients for 342, 684, and 1025 [rpm] were determined to be 27.4, 40.8, 53.3 [$\mathrm{W\,m^{-1}\,K^{-1}}$], respectively. Using the external convection terms and results from open rotor testing, the internal convection heat transfer coefficients for 342, 684, and 1025 [rpm] were determined to be 27.0, 52.7, and 78.3 [$\mathrm{W\,m^{-1}\,K^{-1}}$], respectively. Although based on a small sample population, it was inferred that for the range of speeds tested, the internal convection increases linearly with speed.

While internal and external convective heat transfer coefficients were comparable at 342 [rpm], the internal coefficient increased much more rapidly with increasing speed. This result illustrates the importance of vented rotors for operation at moderate speeds. In terms of the total convective heat transfer, internal convection contributed 45.5% at 342 [rpm], increasing to 55.4% at 1025 [rpm].

To validate the external convective heat transfer, the analytical solution was evaluated for a solid rotating disk. The values attained using the analytical solution were 12.7% lower than the experimental result at 342 [rpm] increasing to 22.3% at 1025 [rpm]. This deviation was largely attributed to the simplicity of the analytical solution.

PIV was used to quantify flow through the internal passage for the same nominal speeds used in the heat transfer experiment. The resulting velocity fields for each speed exhibited similar characteristics, with the exception of the radial velocity which increased with speed. The velocity field showed the presence of a recirculation region on the suction side of the fin, acting to reduce the mean flow rate and convective heat transfer at the suction surface. The pressure side exhibited a dominant radial velocity, suggesting that convection was preferential at that surface. Using the velocity data near the exit of the passage, the volume rates for 342, 684, and 1025 [rpm] were calculated to be 0.0074, 0.0156, and 0.0212 [$\mathrm{m^3\,s^{-1}}$], respectively. As with the internal heat transfer coefficients, it was inferred that the volume flow rate varies linearly with rotor speed. Also, it was established that while a relationship exists between internal heat transfer coefficients and volume flow rate, it does not guarantee a direct relationship.

Observing the TKE of the flow, all three speeds exhibit similar characteristics, varying only in magnitude. The generation of a TKE core was evident along the leading edge of the recirculation region. Addressing the limited expansion of the TKE core and the void of TKE in the recirculation region would serve to enhance internal convection.

With a wealth of experimental heat transfer and flow data, an accurate numerical model could be created to further understand the fin convection mechanism. Furthermore, the idealized numerical model could be extended to predict in-vehicle performance. Conducting this analysis would permit the localized assessment of heat transfer with the potential to improve overall performance.

References

[1] R.G. Dubensky, Experimental techniques for rotor performance measurements, SAE Technical Paper 850078.
[2] A.E. Sisson, Thermal analysis of vented brakerotors, SAE Technical Paper 780352.
[3] A.R. Daudi, 72 curved fin rotor design reduces maximum rotor temperature, SAE Technical Paper 1999-01-3395.
[4] D. Parish, D. MacManus, Aerodynamic investigations of ventilated brake discs, Proceedings of the I MECH E Part D, Journal of Automobile Engineering 219 (4) (2005) 471–486.
[5] J.J. Zhang, A methodological process for optimizing brake cooling and simulation of brake rotor flow field, SAE Technical Paper 952696.
[6] J.J. Zhang, A high aerodynamic performance brake rotor design method for improved brake, SAE Technical Paper 973016.
[7] D. Phan, D. Kondyles, Rotor design and analysis; a technique using computational fluid dynamics (CFD) and heat transfer analysis, SAE Technical Paper 2003-01-3303.
[8] R.A. Jones, P.L. Cormier, T.I.-P. Shih, Modeling the cooling of an automotive brake rotor, SAE Technical Paper 951116.
[9] F.Z. Shen, D. Mukutmoni, K. Thorington, J. Whaite, Computational flow analysis of brake cooling, SAE Technical Paper 971039.
[10] F.P. Incropera, D.P. Dewitt, Fundamentals of Head and Mass Transfer, fourth ed., John Wiley & Sons, Toronto, Canada, 1996.
[11] E.M. Sparrow, J.L. Gregg, Heat transfer from a rotating disk to fluids of any Prandtl number, Journal of Heat Transfer 81 (1959) 249–251.
[12] R. Eisengraber, J. Grochowicz, M. Schuster, K. Augsburg, L. Koch, Comparison of different methods for the determination of the friction temperature of disc brakes, SAE Technical Paper 1999-01-0138.
[13] D.A. Johnson, B.A. Sperandei, R. Gilbert, Analysis of turbulent flow and separation in a vented rotor, ASME Journal of Fluids Engineering 125 (2003) 979–986.
[14] S.B. Pope, Turbulent Flows, Cambridge Univ. Press, Cambridge, UK, 2000.